ACS Photonics

Article

pubs.acs.org/journal/apchd5

Nanophotonic Organic Solar Cell Architecture for Advanced Light Trapping with Dual Photonic Crystals

Akshit Peer[†] and Rana Biswas*[,†,‡]

[†]Department of Electrical and Computer Engineering, and Microelectronics Research Center and [‡]Ames Laboratory, and Department of Physics and Astronomy, Iowa State University, Ames, Iowa, United States

Supporting Information

ABSTRACT: Organic solar cells have demonstrated rapidly increasing efficiencies, but typically absorb less than half of the incident solar spectrum. To increase broadband light absorption, we rigorously design experimentally realizable solar cell architectures based on dual photonic crystals using scattering matrix simulations. There is a polymer microlens on the glass coupled with a photonic-plasmonic crystal at the metal cathode on the back of the cell. The microlens focuses light on the periodic nanostructure that in turn strongly diffracts light. Waveguiding modes and surface plasmon modes enhance long wavelength absorption. The optimal architecture has a period of 500 nm for both arrays, resulting in absorption enhancement of 49% and photocurrent enhancement of 58% relative to the flat cell, for nearly lossless metal cathodes. The enhanced absorption approaches the Lambertian limit. Misalignment between the two photonic crystals leads to about 1% loss of performance. Simulations incorporating experimental dielectric functions for metal cathode and ITO, using a real space methodology find the enhancement of 38% for the photocurrent and 36% for the weighted absorption due to parasitic losses mainly in the metal cathode. This solar architecture is particularly amenable for fabrication since it does not require spin coating of organic layers on corrugated surfaces, but instead requires nanoimprinting an organic layer, followed by metal cathode deposition. This dual photonic crystal architecture has great potential to achieve >12% efficient single junction organic solar cells and to control photons by focusing light on nanostructures and plasmonic components.

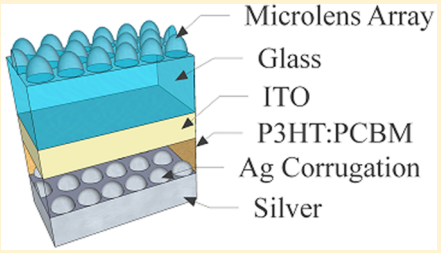

KEYWORDS: *organic solar cell, light trapping, diffraction, surface plasmons*

Organic solar cells (OSCs) have exhibited enormous progress with their power conversion efficiencies increasing from ∼4% just 10 years ago to 11% recently[1] using novel low band gap polymers and tandem solar cells.[2,3] With these rapid advances, organic solar cells may overtake thin film amorphous silicon-based cells. The preferred architecture of organic absorber layers is a bulk heterojunction, with an intimate blend of donor and acceptor material. Photocurrent generation involves photon absorption, exciton formation, exciton diffusion, and dissociation at donor−acceptor interfaces, leading to charge separation and transport of electrons in the acceptor and holes in the donor, under internal electric fields to their respective electrodes.

Organic absorbers are limited in thickness[4] to ensure efficient carrier collection and to minimize carrier recombination, leading to thicknesses of ∼200 nm for prototypical P3HT-PCBM blends and ∼90−100 nm for the lower band gap PTB7 layers. At such thicknesses the absorption of light is incomplete both at long wavelengths (>600 nm) as well as at shorter wavelengths (<450 nm). Utilizing measured wavelength-dependent refractive indices,[5] photon absorption lengths are larger than the absorber layer thicknesses (Figure 1). Consequently, more than half of the incident solar photon flux is not absorbed.

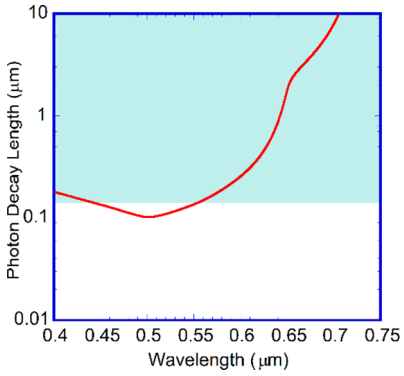

Figure 1. Decay length of photons as a function of wavelength utilizing measured wavelength-dependent refractive indices $n + ik$[5] for the P3HT-PCBM blend. The blue color illustrates the regions where photon decay length exceeds 150 nm, a typical absorber layer thickness.

Various light management strategies using photonic and plasmonic structures have been proposed and studied for enhancing OSCs. One approach utilizes the metal nanoparticle

Received: April 17, 2014
Published: August 15, 2014

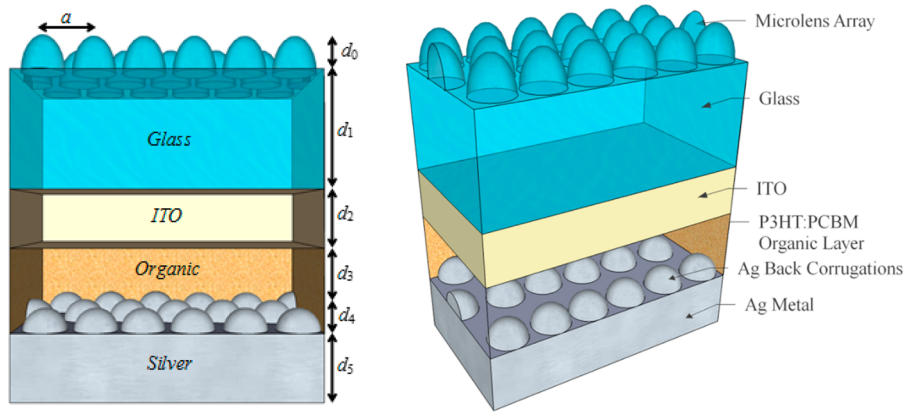

Figure 2. Schematic of the solar cell architecture. The heights of various layers are shown by the d_n, where n denotes the subscript for the particular layer. The pitch of the microlens as well as the photonic crystal array is a. The figure is not drawn to scale.

(NPs) arrays in the electrode or absorber layer[6−14] to generate surface plasmon polaritons (SPPs) within the active layer. SPPs scatter light and enhance the electric field strongly in the active layer, thereby leading to increased light absorption. The incorporation of gold nanoparticles in the PEDOT/PSS as well as the absorber layer improved the efficiency of the polymer solar cell by ∼22%,[15] whereas Ag NPs in the PEDOT layer[16] enhanced efficiency from 6.4 to 7.6% (18% gain) in PCDTBT, through forward scattering effects of the NPs. Recently, organic absorber layers patterned with a one-dimensional metal-grating back electrode showed an increase in the efficiency from ∼7.2 to 7.73% due to field enhancement and scattering.[17] Simulations predicted ∼23% absorption enhancement by patterning the organic absorber layer together with two-dimensional metal gratings.[18] OSCs on wrinkled substrates showed 47% enhancement of photocurrent with a 6-fold enhancement of quantum efficiency at long wavelengths[19] due to light-trapping.[20] A microlens combined with self-aligned microapertures increased the photocurrent from OSCs by 25%[21] by light-trapping.

We recently simulated a fully conformal organic solar cell with a periodically textured indium tin oxide (ITO) or PEDOT layer followed by organic layers and a cathode that conform to this textured substrate.[22] Such a conformal solar cell showed an absorption enhancement of 40% and a current enhancement of 50% for typical thicknesses (150−200 nm) of P3HT-PCBM layers. Although this prediction is very encouraging, there are severe practical problems to achieving such conformal cells. Spin coating an organic layer on a corrugated substrate is very challenging since material preferentially accumulates in the troughs of the structure.[23] Approaches to overcome this problem include reducing the corrugation height or increasing the pitch, but these reduce enhancement from optimal values.

We propose in this paper a more practical approach to light trapping in OSCs than the previous conformal solar cell.[22] Polymer microlens arrays can be readily fabricated by interference lithography[24] and positioned on the top of the glass substrate without altering the architecture or electrical characteristics of the OSC residing on the opposite face of the glass. Microlens arrays focus and diffract light within OSCs and increase out-coupling from OLEDs.[24] We then couple this microlens array with a periodically patterned organic layer with a periodic metal cathode to substantially enhance the photocurrent. Such patterned organic layers have been achieved by imprinting where a PDMS stamp was used to imprint an organic absorber layer with a one-dimensional pattern. A thin (8 nm) layer of MoO_3 followed by a Ag cathode was grown on this structure resulting in a one-dimensional grating cathode.[17] Two-dimensional gratings, offering higher diffraction enhancement, can be similarly imprinted immediately after spin-coating of the organic absorber. Hence, we investigate the architecture (Figure 2) combining a patterned organic-cathode grating with a microlens on the exterior glass, both of which can be fabricated. The combination of the patterned cathode and the microlens has not been investigated theoretically or experimentally before. We rigorously optimize this solar architecture with simulations to predict a current enhancement of ∼58% for this realizable structure.

MATERIALS AND METHODS

The simulated solar cell architecture (Figure 2) has a thick glass substrate (thickness d_1) whose bottom side is coated with an ITO layer (thickness d_2). A triangular microlens array of conical pillars (height d_0) rests on top of the glass. In practice, there is a thin PEDOT/PSS layer (<30 nm) between the ITO and the organic absorber. We do not include the thin layer in our calculations since the optical properties of this layer are similar to ITO. We coat this with a P3HT-PCBM layer (thickness d_3) and a reflecting silver cathode. The organic−cathode interface has periodic corrugations in the form of conical pillars of base radius R and height d_4 in a triangular lattice. The microlens array and the cathode conical array have the same pitch (a). This architecture is suitable for regular organic solar cells, rather than inverted solar cells.

We use the rigorous scattering matrix (SM) method[22,25,26] where Maxwell's equations are solved in Fourier space, that is, in a basis of plane waves for both polarizations. We divide the solar cell into slices in the z-direction wherein the dielectric function depends periodically on x and y. We obtain the SM for the entire structure by integrating the Maxwell's equations with continuity boundary conditions. The SM yields the total reflectance R (including diffraction), transmittance T (∼0), and absorbance A (=1 − R − T) at each wavelength. This SM technique has advantages over real-space methods of being able to simulate fully 3D geometries, without added memory requirements, since a real space grid is unnecessary. The SM method is fully parallelized, with each frequency being sent to a different processor.[22] We characterize solar architectures by their broad-band weighted absorption $\langle A_w \rangle$, weighted by the

dx.doi.org/10.1021/ph500124q | ACS Photonics 2014, 1, 840−847

AM1.5 solar intensity $dI/d\lambda$, and the idealized short circuit current J_{SC}, where

$$\left\langle A_w \right\rangle = \int_{\lambda_2}^{\lambda_1} A(\lambda)\frac{dI}{d\lambda}d\lambda \quad (1)$$

$$J_{SC} = \frac{e}{hc}\int_{\lambda_2}^{\lambda_2} \lambda A(\lambda)\frac{dI}{d\lambda}d\lambda \quad (2)$$

The spectral range of absorption is from λ_1 = 400 nm to λ_2 = 700 nm appropriate for P3HT-PCBM with a HOMO−LUMO splitting of 1.77 eV. Ideal internal quantum efficiency is assumed in simulations. We employ conical arrays in a triangular lattice, an architecture that yielded high enhancements in thin-Si[26,27] and organic[28] solar cells. Convergence was easily achieved with ∼330 plane waves for each polarization, corresponding to a matrix size of 660. We utilize measured wavelength dependent refractive indices $(n + ik)$ for ITO and Ag.[22] To compute the organic layer absorption only, we neglect ITO absorption, and use nearly ideal loss-less metal.[22,29] By adopting this approach, we consider the absorption of photons only in the active layer. The absorption of photons in any other layer cannot contribute to the photocurrent.

RESULTS

A commensurate solar architecture can be achieved by the microlens array having the same pitch as the patterned organic-cathode interface. A critical factor governing light management and diffraction is the pitch of the structure, which we vary first. For a solar cell with just the microlens on top of the glass substrate and flat internal interfaces within the solar cell, we obtain a maximal enhancement of ∼13% in both the absorption and the photocurrent, with an optimized pitch near 1.7 μm (Figure 3a). The enhancement is significantly smaller for smaller pitch but decreases relatively slowly for larger pitch values. The microlens alone increases the absorption over all wavelengths but the amount of enhancement is limited.

In contrast, when we couple the microlens with a corrugated organic-cathode photonic crystal interface (Figure 2), the enhancement increases dramatically, reaching ∼49% for the weighted absorption and ∼58% for the photocurrent (Figure 3a). The optimal pitch is ∼500 nm, significantly smaller than for the microlens alone. The enhancement factor oscillates with a period near 200 nm, indicative of diffraction, and decreases rapidly for larger pitch, going below the performance for the microlens alone as a exceeds 1400 nm. Large pitch corrugations offer limited enhancement. We used an organic-cathode photonic crystal corrugation height of 90 nm (Figure 2), slightly smaller than the thickness of the uniform portion of the organic layer. The reference flat cells have the same volume of absorber material as in the corrugated cell, corresponding to 176 nm thickness of the flat cell. It should be noted that our all optical model predicts photocurrents which are in reasonable agreement with experimental measurements on flat cells with the same absorber layer thickness. For example, using our model, we predict J_{SC} of 8.66 mA/cm^2 for a 150 nm thick cell, which is in very good agreement with the J_{SC} of 8.7 mA/cm^2 measured in ref 30 for the same cell thickness. The complex refractive index of the organic film does depend on spin coating and preparation conditions, which may lead to deviations from the predictions of our model.

The optimal pitch of 500 nm for the patterned solar cell is consistent with mode-coupling theories[31] that predict the optimal pitch to be slightly smaller than the wavelength region of interest over which light trapping is desired, which is the 600−700 nm wavelength region. The photocurrent enhancement exceeds that of the weighted absorption since the photocurrent preferentially weighs the longer wavelengths (eq 2), where larger enhancements are found. We also find (Figure 3b) that even the periodic corrugations in the organic−cathode interface alone result in enhancement of about 50% in J_{SC} and 40% in $\langle A_w \rangle$, with an optimal $a \sim 500$ nm, indicating that surface plasmons and diffraction from the corrugated cathode are significant in enhancing the present solar cell architecture's performance.

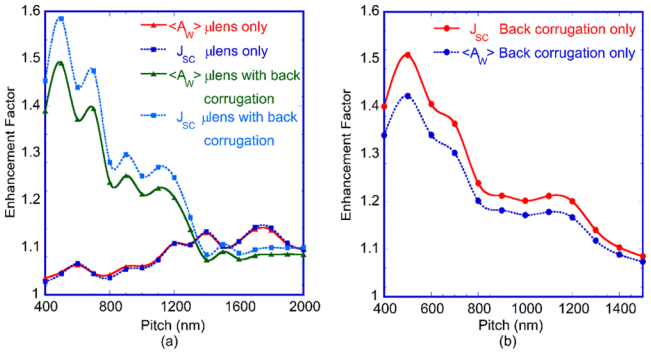

Figure 3. (a) Enhancement in absorption and the photocurrent relative to a flat organic solar cell, as a function of the pitch (i) for the microlens alone and no corrugation in the organic-cathode interface, and (ii) with a microlens combined with photonic crystal array at the organic-cathode interface using a corrugation height of 90 nm in the cathode interface. For the combined array, the optimized microlens height and radii of the microlens as well as the photonic crystal array is 0.3 μm and 0.35a, respectively. For the microlens only case, the optimized microlens height and radii of the microlens is 2.1 μm and 0.40a, respectively. (b) Enhancement in absorption and the photocurrent relative to a flat organic solar cell, as a function of the pitch with only photonic crystal array at the organic−cathode interface using a corrugation height of 90 nm in the cathode interface. The optimized pitch and radii of the photonic crystal array is 500 nm and 0.35a, respectively. The flat portion of the organic layer has a thickness d_3 = 100 nm in both cases. The line through the data points corresponds to the curve fit to guide the eye.

The presence of the microlens is important in determining the enhancement, with the pitch being a critical parameter and the microlens height being less important. The largest photocurrent (J_{SC}) obtained from the present architecture is 13.9 mA/cm^2, corresponding to ∼58% enhancement in J_{SC} and 49% in $\langle A_w \rangle$ (Figure 4). For a fixed organic−cathode corrugation (d_4 = 90 nm), the enhancement factor is relatively flat for microlens heights (d_0) in the range 0.3−1.0 μm. There is a weak minimum for $d_0 \sim 1.3$ μm, although the enhancement becomes nearly constant for larger heights (>1.5 μm). This suggests that, although the microlens height is not a critical parameter in the design, the pitch is critical. This occurs since the pitch of the structure controls the diffraction whereas the lens height may shift the position of the focusing regions within the solar cell structure.

We simulated the weighted absorption as a function of the cone radius (R/a) for a fixed lens height of 0.3 μm (Figure 5). The conical pillars with a base radius R have the highest absorption when $R/a \cong 0.35$. This result is expected from analytic considerations since the scattering potential in this lattice is proportional to $2J_1(GR)/GR$, where J_1 is the first order Bessel function. For the triangular lattice, the lowest reciprocal

dx.doi.org/10.1021/ph500124q | ACS Photonics 2014, 1, 840−847

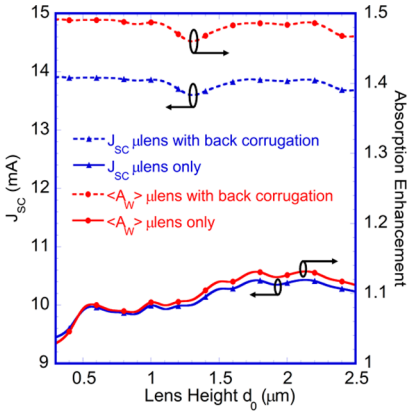

Figure 4. Enhancement in absorption and the photocurrent relative to a flat organic solar cell, as a function of the microlens height d_0 (i) for the microlens alone and no corrugation in the organic−cathode interface, and (ii) with a microlens combined with photonic crystal array at the organic−cathode interface using a corrugation height of 90 nm in the cathode interface. The optimized pitch value of 1700 nm was used for the microlens alone and 500 nm for the combined arrays. The optimized radii (R) of the microlens was 0.4a for the microlens alone and 0.35a in the combined array. The flat portion of the organic layer has a thickness d_3 = 100 nm in both cases. The line through the data points corresponds to the curve fit to guide the eye.

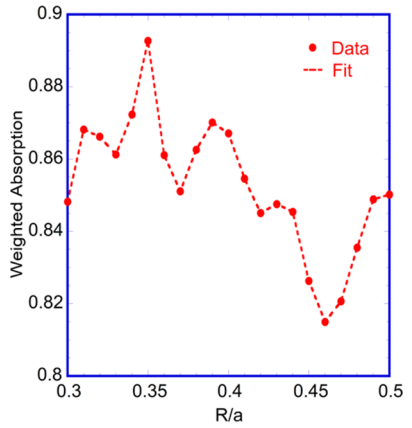

Figure 5. Weighted absorption as a function of R/a for solar cell with 90 nm corrugation in the Ag cathode and microlens of height 0.3 μm. The flat portion of the organic layer has a thickness d_3 = 100 nm and the pitch of the cell is 500 nm. The line through the data points corresponds to the curve fit to guide the eye.

lattice vector is $\mathbf{G_1} = (2\pi/a)(1,-1/\sqrt{3})$ and the largest scattering potential occurs near $R/a \sim 0.35$,[22] corroborating the numerical results. Thus, we choose R/a near 0.35 for all simulations.

We compare the absorption (Figure 6) of the flat and optimally corrugated solar cell (combining the microlens and PC array). We include the Lambertian limit[32] (Figure 6) where light is completely randomized, uniformly populating the photon phase space,[33] and the path length of light is enhanced by a factor of $4n^2$ at each wavelength[34] (n is the λ-dependent refractive index). For organic materials, $4n^2$ is typically 12−15. The optimally corrugated solar cell has enhanced absorption over the flat case at all wavelengths, with largest gains (exceeding 10) at long wavelengths (>600 nm). The absorption of the optimally corrugated cell has a maximum at 460 nm, and approaches the Lambertian limit between 420 and 500 nm and

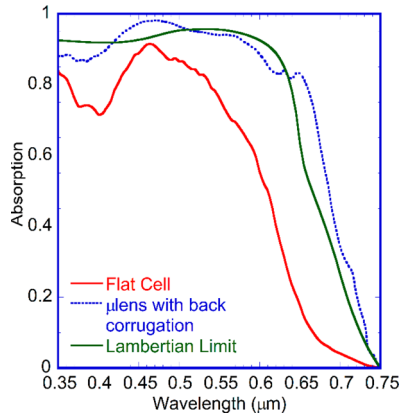

Figure 6. Absorption spectra of (i) a flat cell, (ii) a cell with microlens at the top and corrugation in the cathode, and (iii) the Lambertian limit. The optimized pitch, radii (R) of the microlens as well as the photonic crystal array, and the lens height are 500 nm, 0.35a, and 0.3 μm, respectively.

beyond 640 nm. Moreover, the enhanced absorption can be attributed to the maxima and minima of a dense mesh of resonant wave-guided modes that occur over wavelengths of interest. When the wave-guided modes propagate in the plane of the absorber, the round-trip phase difference from the top and bottom of the absorber layer is a multiple of 2π. The wave-vector perpendicular to the layers is $k_z = m\pi/d$ (d is the absorber layer thickness). For a triangular lattice, any reciprocal lattice vector $\mathbf{G}$ has components $i(2\pi/a)$ and $(2j - i)(2\pi/a)/\sqrt{3}$, respectively, where i and j are integers. Incident light with wave vector $\mathbf{k}_{||}$ is diffracted according to $\mathbf{k}'_{||} = \mathbf{k}_{||} + \mathbf{G}$. Since $k_z = m\pi/d$ and $\mathbf{k}_z^2 + \mathbf{k}_{||}'^2 = n(\lambda)^2(\omega/c)^2$, wave-guiding occurs at resonant wavelengths given by

$$\lambda(i, j, m) = \frac{2\pi n(\lambda)}{\left[\left(i^2 + \frac{1}{3}(2j - i)^2\right)(2\pi/a)^2 + (m\pi/d)^2\right]^{1/2}} \quad (3)$$

where i, j, and m are integers. A dense mesh of wave-guided modes occurs in the long λ region, for our choice of parameters. The phase coherence of waves is assumed at each interface.

Figure 7 illustrates the electric field intensity $|\mathbf{E}|^2$ in the cross section of the solar cell at a typical wavelength of 600 nm for the different optimized solar architectures. In the microlens with a corrugated cathode (Figure 7a), the microlens focuses the field in localized regions within the cell, near the organic−ITO interface, with an enhancement of ~2 in the field intensity. The lateral separation between the intensity maxima is the pitch. Previous ray-tracing simulations confirm focused regions within the absorber for microlenses combined with apertures.[21] As the pitch is increased, the lateral separation of focused spots increases. The microlens focuses light into the absorber layer, which is diffracted by the corrugated cathode. The intensity variations in the absorber also indicate wave-guided modes that propagate in the plane of the structure. Surface plasmons, propagating in the plane of the structure, are generated at the periodically textured metal cathode, resulting in the maximum enhancement in the field intensity by ~2.5 near the organic−metal interface (Figure 7a), at the sides of the conical metal nanopillars, as expected from surface plasmon fields. The lower $n \sim 1.7$ of organics reduces the intensity enhancements as

dx.doi.org/10.1021/ph500124q | ACS Photonics 2014, 1, 840−847

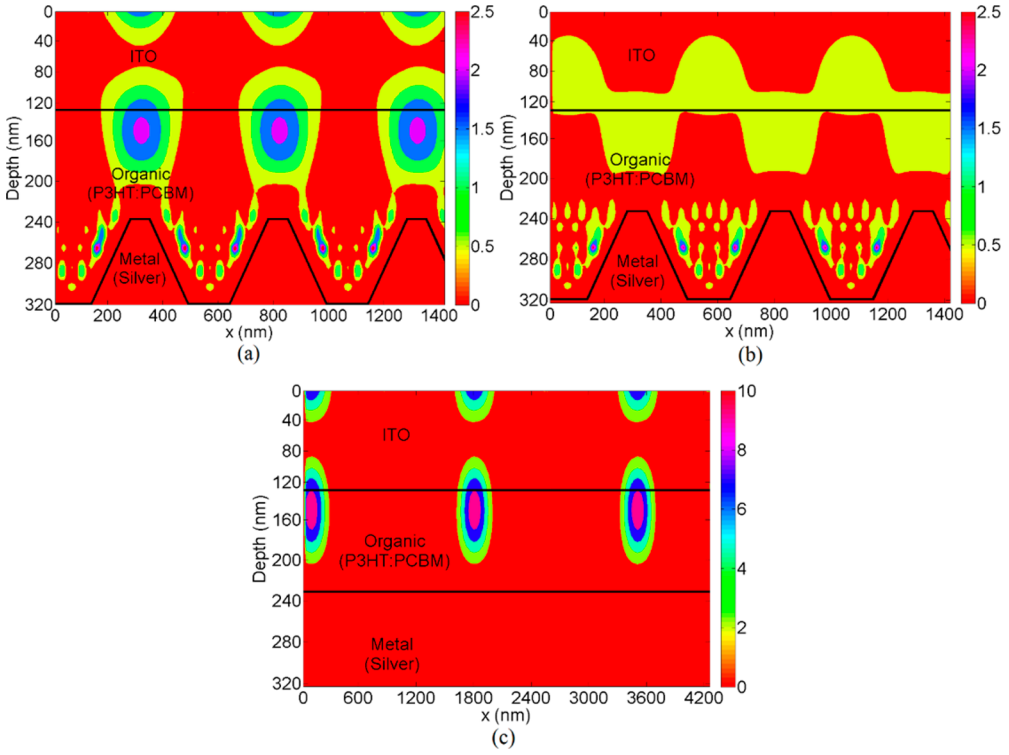

Figure 7. Electric field intensity in the cross-section of the solar cell at 600 nm wavelength (a) with microlens of height 0.3 μm, (b) without the microlens, and (c) with microlens alone (height = 2.1 μm). The optimized pitch value of 1700 nm was used for the microlens alone and 500 nm for the combined arrays. The optimized radii (R) of the microlens was 0.4a for the microlens alone and 0.35a in the combined array.

compared to thin silicon solar architectures with corrugated back reflectors,[26] due to the much higher silicon n (~3.5).

When the organic cathode interface is corrugated without the microlens (Figure 7b), we find surface plasmon formation at this interface without the focusing regions caused by the microlens. The surface plasmons propagate in the plane of the structure generating enhanced absorption. Diffraction from the organic-cathode grating also generates wave-guided modes. For the configuration with only a top microlens array (Figure 7c) and flat solar cell layers, there are narrow highly focused regions where the intensity is enhanced by ~10 within the organic layer, significantly larger than for the microlens with organic−cathode grating. Outside these regions there is no intensity enhancement. Propagating surface plasmons and wave-guided modes are absent.

DISCUSSION

The microlens array produces a succession of standing wave maxima and minima in the underlying dielectric layers, ending with the boundary conditions of vanishing electric field in the metal. The expected separation between nodes (minima) is $\lambda/2n$, which for a free-space λ = 600 nm and a typical organic n ~ 1.7, is ~176 nm. From Figure 7a this separation is ~170 nm, very close to the theoretical prediction. The maxima of the standing waves occur at a separation of $\lambda/4n$ from the metal cathode, which is ~88 nm and located near the interface between the organic and ITO layer.

The fabrication of this architecture requires the microlens to be commensurate with the corrugated cathode, having the same pitch (Figure 2). There could be unavoidable misalignment while experimentally positioning the microlens on the glass. To investigate the effect of lens misalignment on the performance, we simulated the variation in enhancement factor when the microlens array is shifted along a symmetry axis (x-direction) with respect to corrugated organic-metal cathode by varying amounts (Figure 8). Misalignment only reduces the enhancement factor by <1% (Figure 8). The largest misalignment of 250 nm occurs when the top microlens is exactly in the troughs of the corrugated cathode resulting in only ~0.9% decrease in J_{sc} and $\langle A_w \rangle$ in comparison to the perfectly aligned structure. The enhancement ratio is symmetric about the 250 nm shift, due to the structural periodicity (with pitch 500 nm). Hence, the structure is not sensitive to typical fabrication constraints of the thin microlens placement, and the robustness of this design

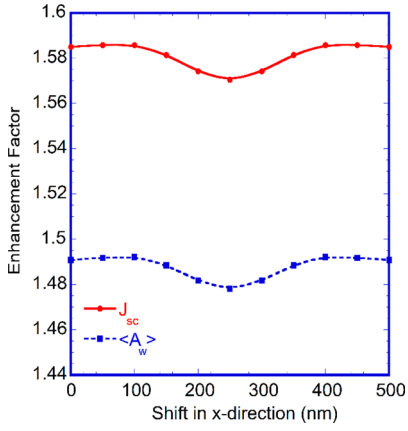

Figure 8. Enhancement in photocurrent and weighted absorption when the microlens is shifted in x-direction with respect to the conical corrugations in the Ag cathode. The optimized values of pitch, radii (R) of the microlens as well as the photonic crystal array, and the lens height are 500 nm, 0.35a, and 0.3 μm, respectively.

dx.doi.org/10.1021/ph500124q | ACS Photonics 2014, 1, 840−847

is appealing for fabrication, an advantage over designs combining microlens arrays with microapertures,[21] where precise alignment is necessary.

The regions of high intensity $|\mathbf{E}|^2$ within the absorber lead to high exciton concentration in locally inhomogeneous regions within the absorber. High exciton densities near the ITO-organic interface promote hole collection at the ITO, whereas excitons near the cathode from surface plasmons benefit electron collection. The quenching of excitons close to the metal cathode has been studied previously. To reduce the exciton quenching near the cathode thin (~10 nm) exciton blocking layers have been employed.[35] Such thin layers will not affect the optical absorption processes studied here. The e- and h-transport is an aspect for further work.

Periodic patterning of conformal thin silicon solar cells has achieved >30% measured enhancements[27] and are a promising direction for organic cells. OSCs on quasi-periodic wrinkled polymer substrates[19] show measured photocurrent enhancements as large as 47% due to light trapping similar to those for periodic structures. Very recently, moth-eye structures with two photonic patterns have shown to enhance the performance of OLEDs.[36] The photocurrent enhancements of 58% found here, imply that the state of the art 8% efficient single junction organic solar cell could be improved to ~12% efficiency with optimal light management, competitive with thin film silicon cells. Light trapping may be employed for tandem organic cells which could increase their efficiency even further, and may lead to >15% efficiency tandem cells, competitive with current thin film technologies.

PARASITIC LOSSES

One of the critical questions is the magnitude of the parasitic losses within (i) the metal cathode and (ii) within the ITO layer, and it is essential to assess whether the enhancements are still valid when all these parasitic losses are accounted for. To address this question, we repeat our calculations for the realistic ITO, as well as the metal cathode where $n_2 = \mathrm{Im}(n) \neq 0$ and is given by experimental measurements. With such calculations, the wavelength dependent absorption $A(\lambda)$ from the optical simulation includes contributions from the ITO and metal cathode. To deconvolute the contribution of the absorption from only the organic material, it is necessary to extract the electric fields $\boldsymbol{E}(\mathbf{r})$ and magnetic fields $\boldsymbol{H}(\mathbf{r})$ in real space by transforming the computed fields in Fourier space. The absorption rate R per unit volume at the position $\mathbf{r}$ is

$$R = \frac{1}{8\pi}\omega \mathrm{Im}(\varepsilon(\omega))|E(r)|^2 \tag{4}$$

The absorption A is then

$$A = \frac{1}{V}\int \frac{4\pi n_1 n_2}{\lambda}|E(x, y, z)|^2 \mathrm{d}x\mathrm{d}y\mathrm{d}z \tag{5}$$

where the integral is only over the organic material of volume V. The absorption is proportional to the imaginary component of the refractive index $n_2 = \mathrm{Im}(n)$. In the mixed grating layer, the sum is only over the organic layer material, a procedure that is computationally intensive since it involves the geometry of the nanocones.

Such a procedure is computationally laborious and not well suited for the present scattering matrix method where Maxwell's equations are solved in Fourier space rather than real space. In fact, such procedures are more amenable to real space solvers such as the finite difference time domain (FDTD) method. The use of Fourier space has great advantages for parallelization and computational efficiency at the expense of not directly calculating the real space fields and separating the losses. Nonetheless, we have implemented this procedure of extracting the real space fields and we separately calculate the losses only in the organic material, with each simulation taking about 1600 CPU hours in a multiprocessor environment utilizing 64 processors.

This procedure yields an enhancement of 38% for J_{SC} and 36% for $\langle A_w \rangle$ for the pitch (a) = 600 nm and R/a = 0.39, the optimum geometry for solar architecture with absorption in the metal and ITO included. This enhancement is somewhat lower than the $(J_{SC}, \langle A_w \rangle)$ enhancement values of (58%, 49%) for the ideal case due to the parasitic absorption in the ITO as well as the metal cathode for both the flat reference and textured cases. We plot the enhancement ratio as a function of the pitch (Figure 9), which shows a maximum for pitch of 600 nm, a trend similar to that for the ideal case (Figure 3). The principal difference is that the peak enhancement at small pitch (600 nm), including parasitic absorption, is lower than the ideal case. Similar to the ideal case, the enhancement factor shows an oscillatory behavior, with a value of ~1.3 for the larger pitch values around 1000−1300 nm. This indicates that structures with a periodicity around 1 μm, which are more amenable to fabrication, provide enhancements near 30% and may also be suitable. As in the ideal case, the enhancement factor decreases for pitch values larger than 1500 nm. Notably, the enhancement of $\langle A_w \rangle$ can be slightly larger than that of J_{SC} for pitch values around 900 nm.

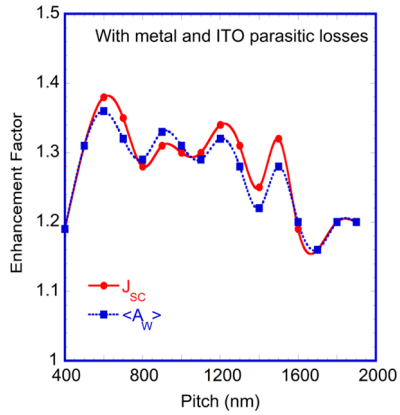

Figure 9. Simulated enhancements as a function of pitch including the losses in both metal cathode and ITO layers. The enhancement in absorption and the photocurrent is relative to a flat organic solar cell, for a solar cell with a microlens combined with photonic crystal array at the organic−cathode interface using a corrugation height of 90 nm in the cathode interface. The optimized microlens height and radii of the microlens as well as the photonic crystal array is 0.3 μm and 0.39a, respectively. The line through the data points corresponds to the curve fit to guide the eye.

By performing calculations with the $\mathrm{Im}(n)$ to be equal to experimental value, we find the ITO absorption to be less than 1% of the total absorption, whereas the parasitic absorption in the metal cathode is much more significant with a value ~10%.

CONCLUSION

The fundamental advance in this paper is that advanced photonic structures can tremendously enhance photon harvesting in organic solar cells through strong diffraction and

dx.doi.org/10.1021/ph500124q | ACS Photonics 2014, 1, 840−847

waveguide modes in conjunction with plasmonic light concentration. We demonstrate experimentally realizable organic solar cell architecture with a periodically textured microlens array on the top of the glass substrate in conjunction with a periodically corrugated metal cathode. This solar architecture is amenable to fabrication since it does not require spin coating of organic layers on corrugated surfaces. It instead requires imprinting an organic layer, followed by metal cathode deposition. The optimized architecture has a period of 500 nm for both arrays, resulting in absorption enhancement of 49% and photocurrent enhancement of 58% relative to the flat cell, with much enhanced absorption at long wavelengths. The absorption approaches the Lambertian limit. By performing the simulations for realistic metal and ITO by a real space methodology, the enhancement was 38% for photocurrent and 36% for weighted absorption due to parasitic losses mainly in the metal cathode. The high enhancement in absorption can be attributed to the patterned metal cathode that diffracts light and generates propagating surface plasmons, which enhance the field intensity at the organic−metal interface. The microlens at the top of the glass substrate focuses the light within the organic absorber layer and further enhances the plasmonic effects. The present solar cell architecture is a unique and practical way to control the light interaction with nanostructures and it has great potential to achieve >12% efficiency for single junction organic solar cells.

■ ASSOCIATED CONTENT

Supporting Information

Wavelength-dependent complex refractive index values of the P3HT-PCBM blend used in the simulation. This material is available free of charge via the Internet at http://pubs.acs.org.

■ AUTHOR INFORMATION

Corresponding Author

*E-mail: biswasr@iastate.edu.

Notes

The authors declare no competing financial interest.

■ ACKNOWLEDGMENTS

This research was partially supported by the Ames Laboratory, operated for the Department of Energy by Iowa State University under Contract No. DE-AC02-07CH11385 (theoretical analysis) and the National Science Foundation through Grant ECCS-1232067 (computational work). The research used resources at the National Energy Research Scientific Computing Center (NERSC), which is supported by the Office of Science of the USDOE under Contract No. DE-AC02-05CH11231. We thank A. Moule for providing experimental data.

■ REFERENCES

(1) You, J.; Dou, L.; Yoshimura, K.; Kato, T.; Ohya, K.; Moriarty, T.; Emery, K.; Chen, C.-C.; Gao, J.; Li, G.; Yang, Y. A polymer tandem solar cell with 10.6% power conversion efficiency. *Nat. Commun.* **2013**, *4*, 1446−1455.

(2) Park, S. H.; Roy, A.; Beaupré, S.; Cho, S.; Coates, N.; Moon, J. S.; Moses, D.; Leclerc, M.; Lee, K.; Heeger, A. J. Bulk heterojunction solar cells with internal quantum efficiency approaching 100%. *Nat. Photonics* **2009**, *3*, 297−303.

(3) Dou, L.; You, J.; Yang, J.; Chen, C.-C.; He, Y.; Murase, S.; Moriarty, T.; Emery, K.; Li, G.; Yang, Y. Tandem polymer solar cells featuring a spectrally matched low-bandgap polymer. *Nat. Photonics* **2012**, *6*, 180−185.

(4) Soga, T. *Nanostructured Materials for Solar Energy Conversion*; Elsevier Science: Amsterdam, 2006.

(5) Moule, A. J.; Meerholz, K. Interference method for the determination of the complex refractive index of thin polymer layers. *Appl. Phys. Lett.* **2007**, *91*, 061901.

(6) Atwater, H. A.; Polman, A. Plasmonics for improved photovoltaic devices. *Nat. Mater.* **2010**, *9*, 205−213.

(7) Kim, S.-S.; Na, S.-I.; Jo, J.; Kim, D.-Y.; Nah, Y.-C. Plasmon enhanced performance of organic solar cells using electrodeposited Ag nanoparticles. *Appl. Phys. Lett.* **2008**, *93*, 073307.

(8) Morfa, A. J.; Rowlen, K. L.; Reilly, T. H., III; Romero, M. J.; van de Lagemaat, J. Plasmon-enhanced solar energy conversion in organic bulk heterojunction photovoltaics. *Appl. Phys. Lett.* **2008**, *92*, 013504.

(9) Duche, D.; Torchio, P.; Escoubas, L.; Monestier, F.; Simon, J.-J.; Flory, F.; Mathian, G. Improving light absorption in organic solar cells by plasmonic contribution. *Sol. Energy Mater. Sol. Cells* **2009**, *93*, 1377−1382.

(10) Shen, H.; Bienstman, P.; Maes, B. Plasmonic absorption enhancement in organic solar cells with thin active layers. *J. Appl. Phys.* **2009**, *106*, 073109.

(11) Vedraine, S.; Torchio, P.; Duché, D.; Flory, F.; Simon, J.-J.; Rouzo, J. L.; Escoubas, L. Intrinsic absorption of plasmonic structures for organic solar cells. *Sol. Energy Mater. Sol. Cells* **2011**, *95*, S57−S64.

(12) Shahin, S.; Gangopadhyay, P.; Norwood, R. A. Ultrathin organic bulk heterojunction solar cells: Plasmon enhanced performance using Au nanoparticles. *Appl. Phys. Lett.* **2012**, *101*, 053109.

(13) Gan, Q.; Bartoli, F.; Kafafi, Z. Plasmonic enhanced organic photovoltaics: Breaking the 10% efficiency barrier. *Adv. Mater.* **2013**, *25*, 2385−2396.

(14) Ouyang, Z.; Pillai, S.; Beck, F.; Kunz, O.; Varlamov, S.; Catchpole, K. R.; Campbell, P.; Green, M. A. Effective light trapping in polycrystalline silicon thin-film solar cells by means of rear localized surface plasmons. *Appl. Phys. Lett.* **2010**, *96*, 261109.

(15) Xie, F.-X.; Choy, W. C. H.; Wang, C. C. D.; Sha, W. E. I.; Fung, D. D. S. Improving the efficiency of polymer solar cells by incorporating gold nanoparticles into all polymer layers. *Appl. Phys. Lett.* **2011**, *99*, 153304.

(16) Baek, S.-W.; Noh, J.; Lee, C.-H.; Kim, B.; Seo, M.-K.; Lee, J.-Y. Plasmonic forward scattering effect in organic solar cells: A powerful optical engineering method. *Nat. Sci. Rep.* **2013**, *3*, 1726.

(17) You, J.; Li, X.; Xie, F.-X.; Sha, W. E. I.; Kwong, J. H. W.; Li, G.; Choy, W. C. H.; Yang, Y. Surface plasmon and scattering-enhanced low bandgap polymer solar cell by a metal grating back electrode. *Adv. Energy Mater.* **2012**, *2*, 1203−1207.

(18) Le, K. Q.; Abass, A.; Maes, B.; Bienstman, P.; Alù, A. Comparing plasmonic and dielectric gratings for absorption enhancement in thin-film organic solar cells. *Opt. Express* **2012**, *20*, A39−A50.

(19) Kim, J. B.; Kim, P.; Pégard, N. C.; Oh, S. J.; Kagan, C. R.; Fleischer, J. W.; Stone, H. A.; Loo, Y.-L. Wrinkles and deep folds as photonic structures in photovoltaics. *Nat. Photonics* **2012**, *6*, 327−332.

(20) Gregg, B.; van de Lagemaat, J. Solar cells: Folding photons. *Nat. Photonics* **2012**, *6*, 278−280.

(21) Tvingstedt, K.; Zilio, S. D.; Inganäs, O.; Tormen, M. Trapping light with micro-lenses in thin film organic photovoltaic cells. *Opt. Express* **2008**, *16*, 21608−21615.

(22) Biswas, R.; Timmons, E. Nano-photonic light trapping near the Lambertian limit in organic solar cell architectures. *Opt. Express* **2013**, *21*, A841−A846.

(23) Nalwa, K. S.; Park, J.-M.; Ho, K.-M.; Chaudhary, S. On realizing higher efficiency polymer solar cells using a textured substrate platform. *Adv. Mater.* **2011**, *23*, 112−116.

(24) Park, J.-M.; Gan, Z.; Leung, W. Y.; Liu, R.; Ye, Z.; Constant, K.; Shinar, J.; Shinar, R.; Ho, K.-M. Soft holographic interference lithography microlens for enhanced organic light emitting diode light extraction. *Opt. Express* **2011**, *19*, A786−A792.

(25) Li, Z.-Y.; Lin, L.-L. Photonic band structures solved by a plane-wave based transfer-matrix method. *Phys. Rev. E* **2003**, *67*, 046607.

(26) Biswas, R.; Xu, C. Nano-crystalline silicon solar cell architecture with absorption at the classical 4n2 limit. *Opt. Express* **2011**, *19*, A664−A672.
(27) Bhattacharya, J.; Chakravarty, N.; Pattnaik, S.; Slafer, W. D.; Biswas, R.; Dalal, V. L. A photonic-plasmonic structure for enhancing light absorption in thin film solar cells. *Appl. Phys. Lett.* **2011**, *99*, 131114.
(28) Nalwa, K. S.; Chaudhary, S. Design of light-trapping microscale-textured surfaces for efficient organic solar cells. *Opt. Express* **2010**, *18*, 5168−5178.
(29) Zhou, D.; Biswas, R. Photonic crystal enhanced light-trapping in thin film solar cells. *J. Appl. Phys.* **2008**, *103*, 093102.
(30) Bhattacharya, J.; Mayer, R. W.; Samiee, M.; Dalal, V. L. Photo-induced changes in fundamental properties of organic solar cells. *Appl. Phys. Lett.* **2012**, *100*, 193501.
(31) Yu, Z.; Raman, A.; Fan, S. Fundamental limit of nanophotonic light trapping in solar cells. *Proc. Natl. Acad. Sci. U.S.A* **2010**, *107*, 17491−17496.
(32) Yablonovitch, E. Statistical ray optics. *J. Opt. Soc. Am.* **1982**, *72*, 899−907.
(33) Schiff, E. A. Thermodynamic limit to photonic-plasmonic light-trapping in thin films on metals. *J. Appl. Phys.* **2011**, *110*, 104501.
(34) Tiedje, T.; Yablonovitch, E.; Cody, G. D.; Brooks, B. G. Limiting efficiency of silicon solar cells. *IEEE Trans. Electron Devices* **1984**, *ED-31*, 711−716.
(35) Peumans, P.; Bulovi, V.; Forrest, S. R. Efficient photon harvesting at high optical intensities in ultrathin organic double heterostructure photovoltaic diodes. *Appl. Phys. Lett.* **2000**, *76*, 2650.
(36) Zhou, L.; Ou, Q.-D.; Chen, J.-D.; Shen, S.; Tang, J.-X.; Li, Y.-Q.; Lee, S.-T. Light manipulation for organic optoelectronics using bio-inspired moth's eye nanostructures. *Nat. Sci. Rep.* **2014**, *4*, 4040.